RSC Advances

PAPER

View Article Online
View Journal | View Issue

Cite this: *RSC Adv.*, 2023, **13**, 2081

Synthesis of a ZSM-5 (core)/SAPO-11 (shell) composite zeolite and its catalytic performance in the methylation of naphthalene with methanol

Xiaoxiao Wang, *[a] Shilong Guo[a] and Ziyan Niu[ab]

Received 25th November 2022
Accepted 2nd January 2023

DOI: 10.1039/d2ra07499k

rsc.li/rsc-advances

In the present work, a ZSM-5 (core)/SAPO-11 (shell) composite was prepared by the hydrothermal method and characterized by X-ray powder diffraction (XRD), scanning electron microscopy (SEM), Fourier transform infrared spectroscopy (FT-IR), temperature programmed desorption of ammonia (NH_3-TPD), and other characterization techniques. The catalytic performance of ZSM-5/SAPO-11 for the methylation of naphthalene with methanol was also studied. For comparison, the mechanical mixture was prepared through the blending of ZSM-5 and SAPO-11. The experimental results showed ZSM-5/SAPO-11 has been prepared with good crystallization, and exhibited a core–shell structure, with the ZSM-5 phase as the core and the SAPO-11 phase as the shell. The pore size of ZSM-5/SAPO-11 was between that of ZSM-5 and SAPO-11, and it had fewer acid sites than ZSM-5 and the mechanical mixture but more acid sites than SAPO-11. The excellent catalytic performance of ZSM-5/SAPO-11 was due to suitable pore size and acidity. The formation mechanism of the ZSM-5/SAPO-11 composite zeolite was also discussed.

2,6-Dimethylnaphthalene (2,6-DMN) is a crucial chemical for the production of high-performance polyester resins such as polyethylenenaphthalate (PEN) and polybutylene naphthalate (PBN). Compared with poly(ethylene terephthalate) (PET), PEN shows superior properties such as higher gas barrier, tensile strength, heat resistance and stability against UV light and X-rays. It possesses applications in different fields such as electronics components, refillable bottles, advanced photo systems, food containers, aviation, and so on.[1,2] PBN is a high-performance aromatic polyester resin, which exhibits excellent anti-abrasion, low friction properties, superior chemical resistance and outstanding gas barrier characteristics. And mainly uses for electronics, insulators and car.[3,4] However, PEN and PBN have not been widely used in the industrial application due to high cost and low availability of 2,6-DMN.

At present, 2,6-DMN is mainly produced by BP-Amoco through four-step reactions from *o*-xylene and butadiene. However, this synthetic route is environmentally unfriendly and expensive, this greatly limits its application in industry.[5] In order to establish a simple and "green" synthesis route of 2,6-DMN with fewer reaction steps and less reaction waste, there are many ways to produce 2,6-DMN.[6–10] In view of the abundant resources of naphthalene and methanol in China, the synthesis of 2,6-DMN by the methylation of naphthalene with methanol over zeolites has been selected as the preferred route due to its simple technological process and low production cost. The key role of the process is to find a zeolite catalyst with high selectivity of 2,6-DMN at acceptable conversion of naphthalene. The catalyst should possess moderate acidity and suitable pore size because the products of the methylation are very complicated and dimethylnaphthalene (DMN) has 10 different isomers with similar boiling point. It is very difficult to separate 2,6-DMN from 2,7-DMN due to the very tiny difference in boiling point of only 0.3 °C.[11]

Recently, the methylation of naphthalene has been studied over some zeolites catalysts such as ZSM-5, HY, mordenite, SAPO-11 and Hβ.[12–15] Among them, SAPO-11 and ZSM-5 zeolites catalysts were the most widely studied catalysts for the methylation of naphthalene with methanol. SAPO-11 is a member of the silico-aluminophosphate (SAPO-n) family which was firstly synthesized by Union Carbide Corporation. It has a milder acidity and has a one-dimensional pore molecular sieve with pore size of 0.39 nm × 0.63 nm (between the pore size of large-pore and medium-pore zeolites).[16,17] The pore size of SAPO-11 is larger than 0.60 nm, which can sieve effectively the products of naphthalene methylation and decreases further transport resistance that would increase the selectivity of 2,6-DMN. In addition, SAPO-11 shows excellent resistance to deactivation by carbonaceous deposits due to its one-dimensional pore, but unfortunately SAPO-11 has low high initial naphthalene conversion because of its relatively weak acidity. ZSM-5 is an MFI structure possessing intersecting three-dimensional (3D) channels, including straight channels (5.1 × 5.5 Å, 10-membered ring), sinusoidal channels (5.3 × 5.6 Å, 10 MR), and

[a]*College of Chemical Engineering and Technology, Shanxi Key Laboratory of High Value Utilization of Coal Gangue, Taiyuan University of Science and Technology, Taiyuan, PR China. E-mail: xxwang@tyust.edu.cn*
[b]*WuXi AppTec (Tianjin) Co., Ltd., Tianjin, PR China*

intersections (~9 Å).[18–21] In comparison, ZSM-5 gives low selectivity of 2,6-DMN but high initial naphthalene conversion due to its large pore size and strong acidity. Therefore, considerable effort has been devoted to develop suitable catalysts with moderate acidity, pore size and good mechanical stability to combine both advantages and to avoid both disadvantages of SAPO-11 and ZSM-5.

There is a common belief that composite zeolite with binary structure not only combine the advantages of the two distinct kinds of molecular sieve, but also induce the formation of special properties which can improve its catalytic performance.[22] Zhang *et al.* synthesized Y/MCM-48 composite zeolite and found that the composite material exhibited both properties of mesoporous MCM-48 and microporous Y zeolites. Compared with MCM-48 zeolite, Y/MCM-48 composite zeolite showed a higher hydrothermal stability, which resulted in its thicker pore-wall, and stronger acidity.[23] Chae *et al.* developed ZSM-5/SAPO-34 composite catalysts to control the composition of light olefins in MTO reaction. The experimental results showed that a series of composite catalysts synthesized by successive crystallization of SAPO-34 synthetic gel after ZSM-5 crystallization exhibited relatively high catalytic performance.[24] Zhang *et al.* prepared SAPO-11/Hβ composite zeolite with hydrothermal method. For comparing, the mechanical mixture of SAPO-11 and Hβ was also prepared by fully blending. The results indicated that the properties and catalytic performance of the composite was quite different from those of the mechanical mixture, which was due to the occurrence of the strong interaction of SAPO-11 and Hβ in the composite.[25] Wang *et al.* synthesized MAZ/ZSM-5 composite zeolite and studied its catalytic performance in FCC gasoline aromatization. The catalytic evaluation results showed that the composite zeolite had a good performance in FCC gasoline aromatization reactions.[26]

Therefore, in this paper, a combination of ZSM-5 and SAPO-11 might give rise to optimal catalyst to meet a change of market demand for PEN and PBN. Therefore, the ZSM-5 (core)/SAPO-11 (shell) composite zeolite was synthesized through hydrothermal method. For comparison, the mechanical mixture was prepared through the blending of ZSM-5 with SAPO-11. The physicochemical properties of ZSM-5, SAPO-11, the composite and the mechanical mixture were characterized by XRD, SEM, TEM, FT-IR, N_2 adsorption–desorption and NH_3-TPD, and their catalytic performances of these samples were also studied for the methylation of naphthalene with methanol.

Experimental

Catalyst preparation

ZSM-5 was synthesized by a hydrothermal method from a gel molar composition of 0.2template:SiO_2:0.02Al_2O_3:0.09Na_2-O:35H_2O. Tetraethyl orthosilicate (TEOS) (40 wt% SiO_2) and sodium aluminate (80 wt% Al_2O_3) were used as source of Si and Al, tetrapropylammonium hydroxide (TPAOH) was used as the template. The gel mixture was transferred into a stainless steel autoclave, heated in an oven at 200 °C for 24 h. The product thus obtained was washed, dried at 120 °C for 12 h, and calcined in air at 550 °C for 6 h to remove the template completely.

SAPO-11 was synthesized from synthetic gel composition 1.0Al_2O_3:1.0P_2O_5:0.6SiO_2:1.2template:49H_2O. Pseudoboehmite

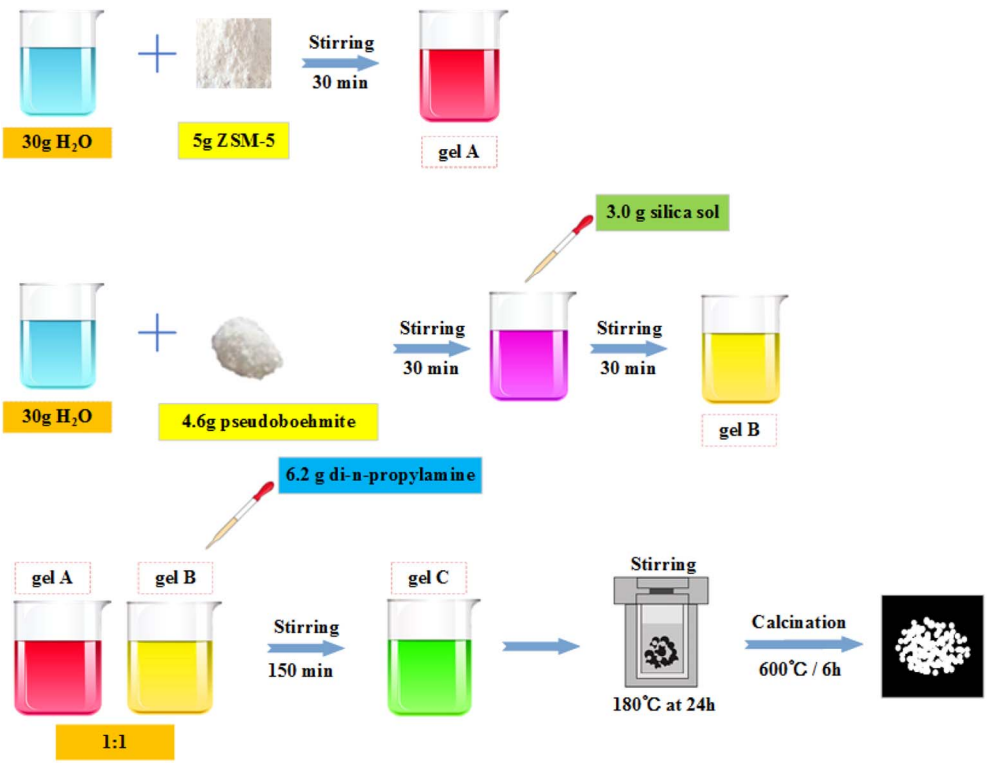

Fig. 1 Schematic of the typical synthesis procedure of ZSM-5/SAPO-11 zeolite catalyst.

(72 wt% Al_2O_3), orthophosphoric acid (85% H_3PO_4) and silica sol (30 wt% SiO_2) were used as source of Al, P and Si. Di-*n*-propylamine (99 wt%) was used as the template. The final crystallization temperature of 180 °C and crystallization time of 24 h was employed. The as-synthesized samples were washed with distilled water, then dried at 120 °C for 12 h and calcined at 600 °C for 4 h.

ZSM-5/SAPO-11 zeolite catalyst was synthesized *via* hydrothermal approach and the step was as follows: (1) 5 g of ZSM-5 powder was added to 30 g of distilled water and stirred for 30 min to form gel A. (2) 7.8 g of orthophosphoric acid (85% H_3PO_4) was added to 70 g of distilled water and the mixture was stirred for 30 min. Then, 4.6 g of pseudoboehmite (72 wt% Al_2O_3) was added dropwise and the mixture was stirred for another 30 min. Afterwards, 3.0 g silica sol (30 wt% SiO_2) was added dropwise with further stirring for 120 min to get a homogeneous gel B. (3) 6.2 g of di-*n*-propylamine (99 wt%) was added to the mixture of gel A and B (1 : 1). The mixture was stirred for 150 min to form homogenous gel C. (4) Gel C was transferred to a stainless steel autoclave and heated to 180 °C for 24 h to produce the solid production. Then the solid production was washed with distilled water and dried at 120 °C overnight. At last, the solid production was calcinated at 600 °C for 6 h to remove the templates in the pores of the sample. In this way, the ZSM-5/SAPO-11 zeolite was obtained. In addition, the mass ratio of ZSM-5 to SAPO-11 was about 1 : 1 in the sample of ZSM-5/SAPO-11. The preparation procedure was schematically depicted in Fig. 1.

For comparison, the mechanical mixture of ZSM-5 and SAPO-11 were prepared by blending of ZSM-5 (self-made) with SAPO-11(self-made) (the mass ratio of ZSM-5 to SAPO-11 was 1 : 1) and was named as ZSM-5 &SAPO-11 zeolite.

Catalyst characterization

X-ray powder diffraction (XRD) analysis was carried out on D/max-2500 X-ray diffractometer of Rigaku Company in Japan. Diffraction patterns were recorded with Cu Kα radiation at 40 kV and 100 mA in the scan range between 5° and 90° to identify the phase structure of the sample. The data was automatically collected by the computer.

Scanning electron microscopy (SEM) was performed with a LEO-435VP scanning electron microscopy operated at 20 kV and 50 PA.

High-resolution transmission electron microscopy (TEM) was carried out to further characterize the microstructure of the samples. The samples were prepared as follows: a small amount of the examined materials was carried out in 1.25 cm^3 of ethanol. A few drops from this suspension were deposited and dried onto the surface of the grid (CF 200 Cu TEM grid).

The textural properties of the samples were derived from N_2 adsorption–desorption measurement on Micromeritics Tristar 3000. In each case, the sample was outgassed under vacuum at 300 °C for 3 h before N_2 adsorption. The specific surface area was calculated according to BET method and the volume of porous were also obtained by t-plot analysis of the adsorption isotherm.

Fourier transform infrared (FTIR) spectroscopy spectra of the samples were obtained using a Nicolet 380 FTIR spectrometer. Scan from 4000 cm^{-1} to 400 cm^{-1} with a resolution of 4.0 cm^{-1}.

The acidity was examined by temperature programmed desorption of ammonia (NH_3-TPD) techniques, which was carried out in a flow system with a thermal conductivity detector. All samples were preheated from room temperature to 500 °C in argon flow and kept at 500 °C for 1 h, which was followed by NH_3 saturation in a flowing NH_3/Ar stream at 40 °C for 5 min. Evacuation at 40 °C for 40 min was carried out to remove physically adsorbed NH_3 then the catalyst was heated to 600 °C at a linear heating rate of 10 °C min^{-1}, and the detector signal of NH_3 was recorded.

Catalyst evaluation

The experiments were performed in a continuous flow fixed-bed reactor equipped with 20 mm diameter and 600 mm length stainless steel tube. 2.5 g of 20–40 mesh zeolite catalysts were loaded in the reaction tube. The reaction mixture was fed into the reactor by a quantity measuring pump and the pressure was kept by N_2. The weight hourly space velocity (WHSV) of naphthalene was 0.19 h^{-1} in all experiments. The reaction temperature was 400 °C and the liquid reactant including naphthalene, methanol and mesitylene (solvent) in a molar ratio of 1 : 5 : 3.5 was preheated before passing to the reactor. The reaction products were analyzed by gas chromatography (GC9560) with a Beta-Dex120 capillary column. The conversion of naphthalene was calculated as follows:

$$\text{Naphthalene conversion } (\%) = \left(\frac{n_{N,0} - n_N}{n_{N,0}}\right) \times 100\%$$

where $n_{N,0}$ and n_N are the molar percentage of naphthalene before and after the reaction. The product distribution include the corresponding molar percentages of ethylnaphthalene (EN), methylnaphthalene (MN), dimethylnaphthalene (DMN) and trimethylnaphthalenes (TMN) in the total product mixture.

$$\text{2,6-DMN selectivity } (\%) = \left(\frac{\sum n_{DMN}}{n_N + n_{MN} + n_{DMN} + n_{TMN}}\right) \times 100\%$$

$$\text{2,6-DMN yield} = (\text{naphthalene conversion} \times \text{2,6-DMN selectivity}) \times 100\%.$$

Results and discussion

Characterization of catalysts

XRD. The XRD patterns of ZSM-5, SAPO-11, ZSM-5&SAPO-11 and ZSM-5/SAPO-11 zeolites are shown in Fig. 2. Compared with ZSM-5 and SAPO-11, the typical characteristic peaks of ZSM-5 and SAPO-11 are identified for ZSM-5&SAPO-11 and ZSM-5/SAPO-11, and there are some overlapping forms between the typical characteristic peaks of ZSM-5 and SAPO-11. The typical characteristic peaks at $2\theta = 7.83°$ and 8.66° attributing to ZSM-5

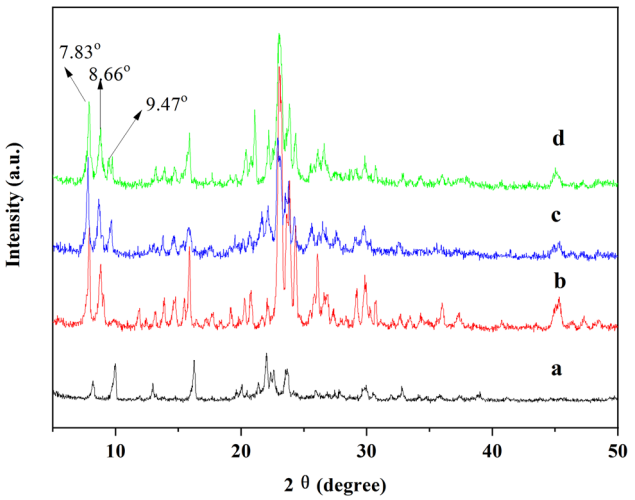

Fig. 2 XRD patterns of synthesized zeolites catalysts (a) SAPO-11; (b) ZSM-5; (c) ZSM-5&SAPO-11; (d) ZSM-5/SAPO-11.

and peak at $2\theta = 9.47°$ attributing to SAPO-11.[27,28] It can be seen that the crystallinity of ZSM-5/SAPO-11 is higher than that of ZSM-5&SAPO-11. Meanwhile, the XRD peak positions shifts slightly to a lower 2θ for ZSM-5/SAPO-11, which is due to the formation of defects and/or lattice contraction in the framework. It indicates that the interaction between SAPO-11 and ZSM-5 can be existed in ZSM-5/SAPO-11 composite zeolite.

SEM. Fig. 3 shows the SEM images of ZSM-5, SAPO-11, ZSM-5&SAPO-11 and ZSM-5/SAPO-11 zeolites. It can be seen that ZSM-5/SAPO-11 shows unique spherical crystal morphology and ZSM-5&SAPO-11 appears disorderly, which indicates that ZSM-5 is embedded in SAPO-11.

TEM. To further observe the combination of ZSM-5 and SAPO-11, the TEM images of ZSM-5/SAPO-11 are provided in Fig. 4. It is obvious that ZSM-5/SAPO-11 is composed of two different types of particles, with ZSM-5 as the core, and SAPO-11 as the shell. These results indicate that ZSM-5 and SAPO-11 are combined uniformly in the composite zeolite.

FT-IR. The FT-IR spectra of synthesized samples are shown in Fig. 5. As shown in Fig. 5a, the bands at 1119 cm^{-1} and 1228 cm^{-1} are assigned to the asymmetric stretching vibration of inner tetrahedra and the asymmetric stretching vibration of outer tetrahedra, respectively.[29] The peaks at 708 cm^{-1} and 754 cm^{-1} are attributed to the symmetric stretching vibration of inner tetrahedra and the symmetric stretching vibration of outer tetrahedra, respectively. The peaks at 630 cm^{-1} and 663 cm^{-1} correspond to the deformation vibration of four-membered ring and the deformation vibration of six-membered ring, respectively. The band at 473 cm^{-1} is due to the flexural vibration of T–O bond. Fig. 5b shows that the peaks at 454 cm^{-1} and 546 cm^{-1} are attributed to the flexural vibration of T–O–T bond of inner tetrahedra and the absorption peak of double bow, respectively. The bands at 1094 cm^{-1} and 796 cm^{-1} are assigned to the asymmetric stretching vibration of outer tetrahedra and the symmetric stretching vibration of outer tetrahedra, respectively. The peak at 1221 cm^{-1} corresponds to the asymmetric stretching vibration of inner tetrahedra.[30] From the Fig. 5, we can see that the bands at 1094 cm^{-1}, 796 cm^{-1}, 542 cm^{-1} and 457 cm^{-1} in the ZSM-5/SAPO-11 zeolite shift to the lower wave number (1092 cm^{-1}, 792 cm^{-1}, 544 cm^{-1} and 454 cm^{-1}), which suggests that there are strong interactions between SAPO-11 and ZSM-5 in the ZSM-5/SAPO-11 composite zeolite.

NH_3-TPD. NH_3-TPD characterization is used to measure the acid strength and acid amount of synthesized samples. The acid strength is determined by the ammonia desorption peak temperature, while the acid amount is estimated by the areas

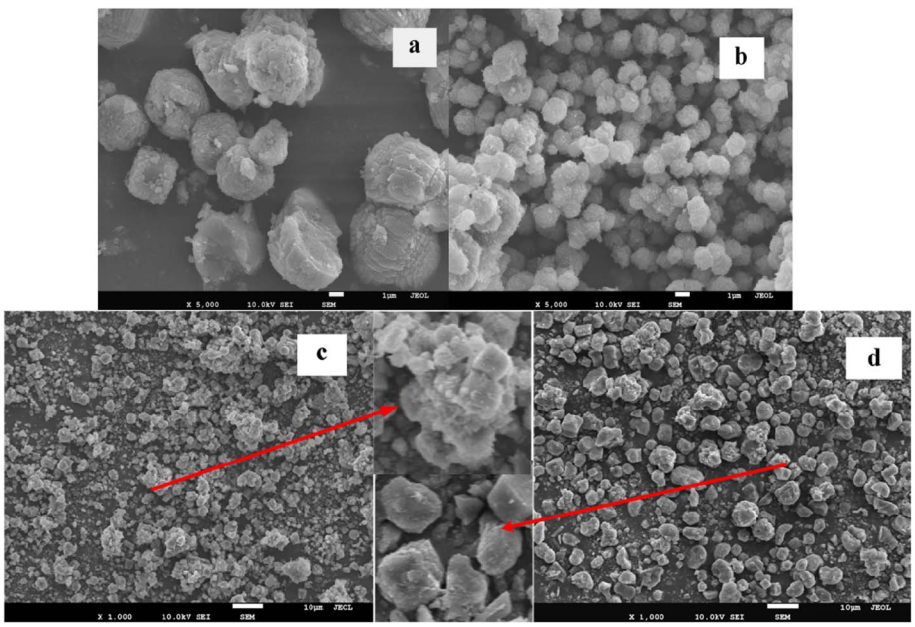

Fig. 3 SEM images of synthesized zeolites catalysts. (a) SAPO-11; (b) ZSM-5; (c) ZSM-5&SAPO-11; (d) ZSM-5/SAPO-11.

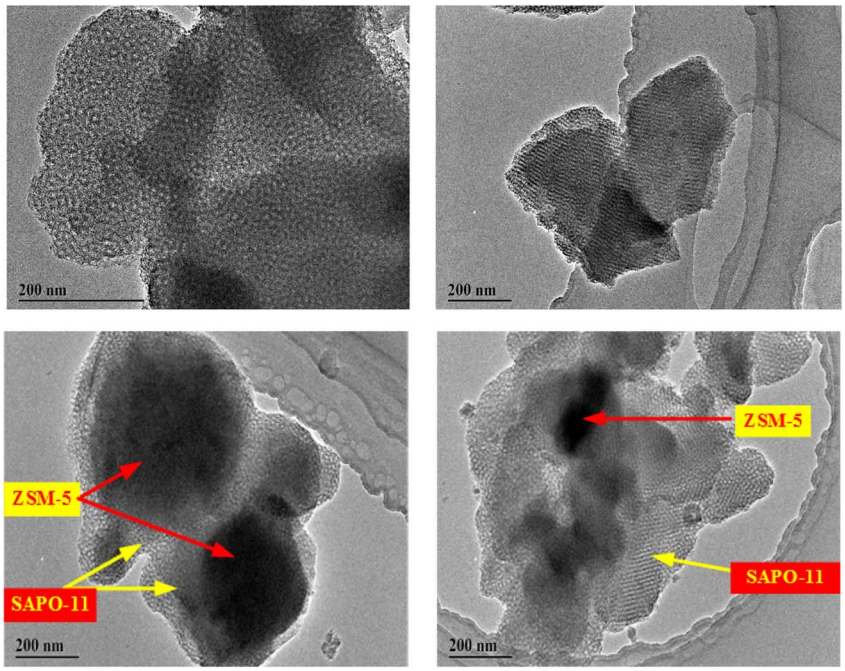

Fig. 4 TEM images of ZSM-5/SAPO-11 composite zeolite.

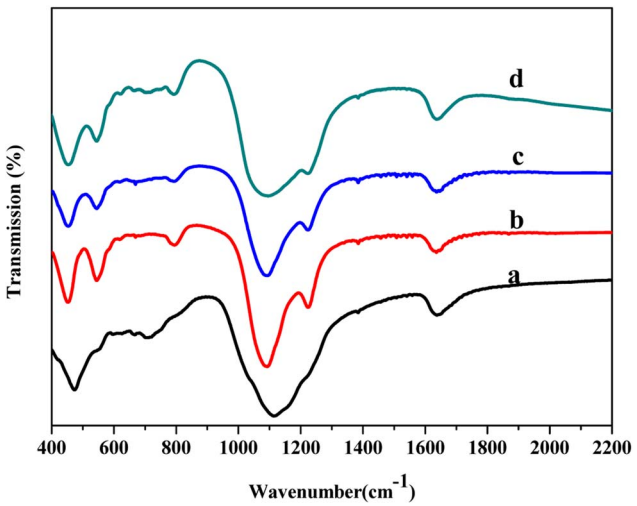

Fig. 5 FTIR spectra of synthesized zeolites catalysts. (a) SAPO-11; (b) ZSM-5; (c) ZSM-5&SAPO-11; (d) ZSM-5/SAPO-11.

under the TPD curves. The NH_3-TPD profiles of four samples are shown in Fig. 6 and their relative amounts and the acidic strength of acid sites are listed in Table 1. There are three NH_3 desorption peaks at about *ca.* 220 °C, 300 °C and 450 °C, corresponding to weak acid sites, medium strong acid sites and strong acid sites. As depicted in Fig. 6, there are two kinds of NH_3 desorption peaks observed in the profile of ZSM-5, indicating that ZSM-5 possesses both the weak acid sites and strong acid sites. However, SAPO-11 exhibits the weak acid sites and medium strong acid sites. Fig. 6 shows that the acid amount of ZSM-5&SAPO-11 decreases compared with ZSM-5 because of ZSM-5 is mixed with SAPO-11, but the peak position of that has not changed. ZSM-5 has the strongest acidity, while SAPO-11 has the weakest acidity. Compares with ZSM-5, the acid amount of ZSM-5&SAPO-11 decreases because ZSM-5 is mixed with SAPO-11, but the peak position of that has not changed. Compared with ZSM-5&SAPO-11, ZSM-5/SAPO-11 exhibits lower acidity, which further indicates the occurrence of strong interaction of ZSM-5 and SAPO-11 in the composite. As shown in Fig. 6 and Table 1, the acid strength and the total acid amount of the acid sites decreases in the order of ZSM-5 > ZSM-5&SAPO-11 > ZSM-5/SAPO-11 > SAPO-11.

Pyridine-IR. Pyridine-IR is used to further evaluate the type (Lewis and Brønsted) of acid sites for all the samples. The

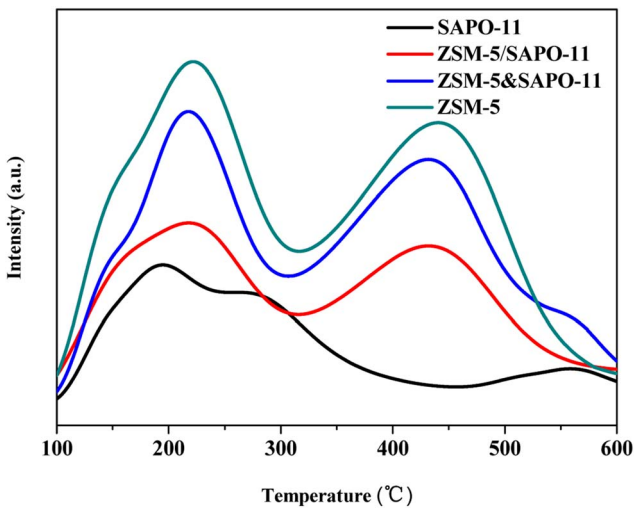

Fig. 6 Results of NH_3-TPD of synthesized zeolites catalysts.

Table 1 Acidity values of different zeolites catalysts

Sample	Weak acid sites		Medium strong acid sites		strong acid sites		The total acid amount (mmol g^{-1})
	Peak temperature (°C)	The acid amount (mmol g^{-1})	Peak temperature (°C)	The acid amount (mmol g^{-1})	Peak temperature (°C)	The acid amount (mmol g^{-1})	
SAPO-11	200	0.54	282	0.48	0	0	1.02
ZSM-5	220	1.36	0	0	440	1.12	2.56
SAPO-11&ZSM-5	220	1.05	0	0	430	0.94	1.99
SAPO-11/ZSM-5	220	0.69			430	0.72	1.42

Brønsted acid sites of synthesized zeolites catalysts could protonate pyridine and form the pyridinium ion, which exhibit the characteristic ring vibrational frequency at 1540 cm^{-1}. As an electron-pair acceptor Lewis aluminum can bind pyridine in a covalent fashion, giving rise to a vibrational band at 1450 cm^{-1}. The relative amounts of Brønsted and Lewis acid sites can be estimated by integration of these two bands after correction for differences in oscillator strengths.[31,32] Table shows that the concentration of Brønsted and Lewis acid sites after pyridine desorption at 200 °C and 400 °C. As shown in Table 2, both the concentration of Brønsted acid sites and Lewis acid sites decrease in the order of ZSM-5 > ZSM-5&SAPO-11 > ZSM-5/SAPO-11 > SAPO-11, indicating that the Brønsted acid sites and Lewis acid sites of synthesized samples decrease in the same order, which is in agreement with the results of NH_3-TPD shown in Fig. 6. Meanwhile, Brønsted acid sites are predominant for all the investigated zeolites catalysts, but the ratio of Brønsted acid sites to Lewis acid sites varies among different catalysts. This may be due mainly to the fact that the acidic sites of molecular sieves, *i.e.*, aluminum species of molecular sieves-framework Al and external-framework Al, change with the synthetic methods and conditions.[33]

Table 2 Brønsted acid sites and Lewis acid sites of synthesized zeolites catalysts of absorbed pyridine

Sample	Brønsted acid sites		Lewis acid sites		Total acid sites	
	200 °C	400 °C	200 °C	400 °C	200 °C	400 °C
SAPO-11	10.25	11.12	2.26	0.56	12.51	11.68
ZSM-5	21.76	18.46	10.20	7.58	29.34	25.92
SAPO-11&ZSM-5	16.20	14.20	7.90	3.43	24.10	17.63
SAPO-11/ZSM-5	13.23	12.68	4.58	2.49	17.81	15.17

N_2 adsorption–desorption. Table 3 presents the pore structure parameters of synthesized samples. As shown in Table 3, most of the pore sizes has a diameter of 0.63 nm and some have diameters of 0.55–0.62 nm. ZSM-5 owns the maximum surface area and pore volume while SAPO-11 owns the minimum surface area and pore volume. Compared with SAPO-11&ZSM-5, ZSM-5/SAPO-11 has larger surface area and pore volume.

The N_2 adsorption–desorption isotherms of synthesized samples are shown in Fig. 7.

The typical N_2 adsorption–desorption isotherms of synthesized samples are of the type IV isotherm according to the IUPAC classification. High adsorption of N_2 occurred in the low

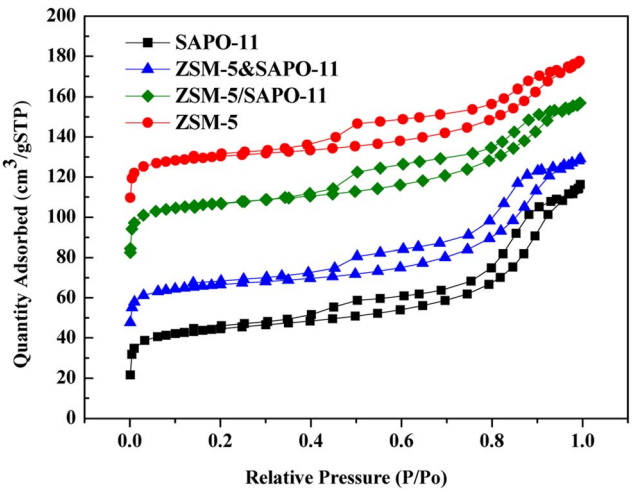

Fig. 7 N_2 adsorption–desorption isotherm plot of synthesized samples.

Table 3 The pore structure parameters of synthesized samples

Sample	Pore size (nm)[a]	Surface area (m^2 g^{-1})			Pore volume (cm^3 g^{-1})		
		BET[a]	Micropore[b]	External	Total[c]	Micropore[b]	Mesopore
SAPO-11	0.55	149	91	58	0.145	0.091	0.054
ZSM-5	0.63	256	172	84	0.187	0.108	0.079
SAPO-11&ZSM-5	0.62	182	106	76	0.163	0.100	0.063
SAPO-11/ZSM-5	0.58	223	124	99	0.172	0.103	0.069

[a] BET method. [b] *t*-Plot method. [c] Volume adsorbed at $p/p_0 = 0.99$.

relative pressure range and obvious hysteresis are detected, suggesting the existence of micropores and the secondary mesopores in all zeolites catalysts. A hysteresis between adsorption and desorption branches is observed at medium relative pressure (0.2–1.0) for all the samples, which demonstrates the presence of a large number of secondary mesopores. These secondary mesopores may be contributed by the filling of interparticle spaces, the particle size being quite uniform.[34] Fig. 7 shows that the secondary mesopores size distributions decreases in the order of ZSM-5 > ZSM-5/SAPO-11 > ZSM-5&SAPO-11 > SAPO-11.

Formation mechanism of ZSM-5 (core)/SAPO-11 (shell) composite zeolite

Formation mechanism of ZSM-5 (core)/SAPO-11 (shell) composite zeolite is shown as follows. The process is shown in Fig. 8. Firstly, ZSM-5 is fixed to orthophosphoric acid by chemical bond. Then, orthophosphoric acid reacts with pseudoboehmite and silica sol to form the colloid (containing Al, P and Si) around the ZSM-5, and di-*n*-propylamine (template) is added to the colloid and reacts with it to form SAPO-11 crystals around ZSM-5. Overall, ZSM-5 is mainly used as seed during the synthesis process, the interaction of ZSM-5 and SAPO-11 maybe is the chemical bond. Then, At last, di-*n*-propylamine (template) is added to the colloid and reacts with it to form SAPO-11 crystals around ZSM-5. Thus, ZSM-5 serves mainly as a seed for the crystallization of the composite during the synthesis process of the composite. And the interaction existed in the SAPO-11 and ZSM-5 maybe refers to the chemical bond between orthophosphoric acid and ZSM-5.

Catalytic performances of the methylation of naphthalene

The conversion of naphthalene of ZSM-5, SAPO-11, ZSM-5&SAPO-11 and ZSM-5/SAPO-11 zeolites catalysts are compared in Fig. 9 at the reaction time of 1 h and 6 h, respectively. As shown in Fig. 9, the highest initial naphthalene conversion of these catalysts follows this order ZSM-5> ZSM-5&SAPO-11 > ZSM-5/SAPO-11 > SAPO-11, which is consistent with the characterization result of NH_3-TPD. This can be attributed to the fact that zeolite catalyst with strong acid acidity exhibit higher initial naphthalene conversion, which provide a large number of active sites for the methylation of naphthalene. Additionally, the conversion of naphthalene of ZSM-5 at the reaction time of 1 h and 6 h is 65.2% and 10.6%, respectively. The conversion of naphthalene for SAPO-11 are 55.2% and 24.5% at the reaction time of 1 h and 6 h individually. And the naphthalene conversion of ZSM-5/SAPO-11 is 58.2% at the reaction time of 1 h, which is lower than that of ZSM-5&SAPO-11 (59.4%), but the naphthalene conversion of ZSM-5/SAPO-11 is 28.3% at the reaction time of 6 h, which is higher than that of ZSM-5&SAPO-11 (25.5%). From Fig. 9, we can see that although ZSM-5/SAPO-11 shows lower initially naphthalene conversion, its stability is higher than that of other catalysts.

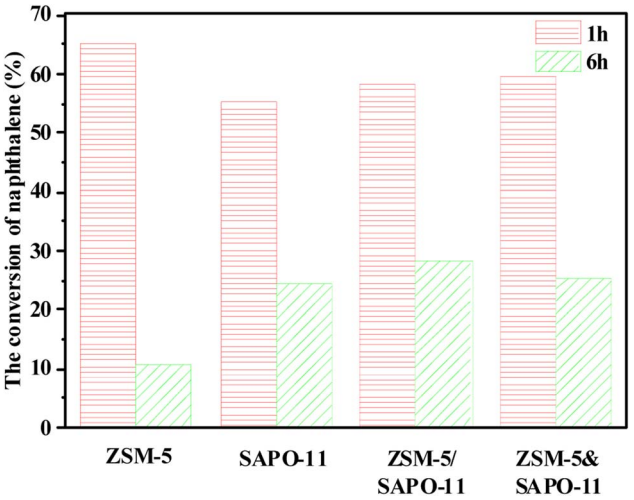

Fig. 9 The conversion of naphthalene of ZSM-5, SAPO-11, ZSM-5&SAPO-11 and ZSM-5/SAPO-11 zeolites catalysts (at the reaction time of 1 h and 6 h).

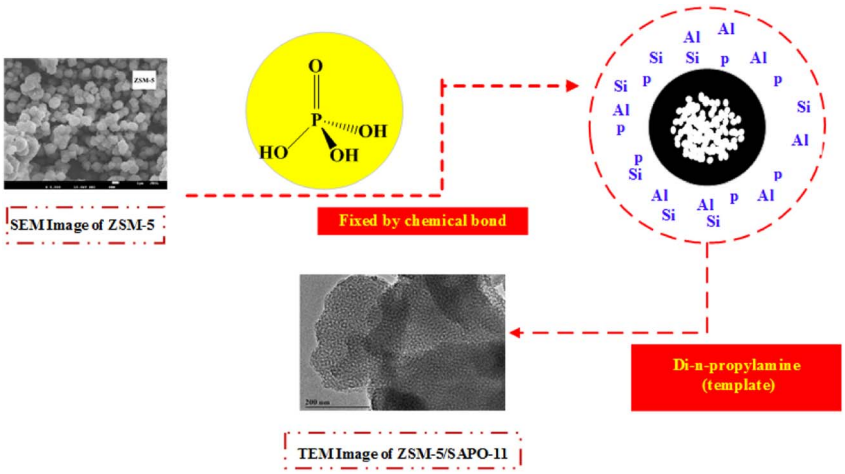

Fig. 8 Formation mechanism of ZSM-5 (core)/SAPO-11 (shell) composite zeolite.

Table 4 Comparison of catalytic performance of synthesized samples in the methylation of naphthalene

Sample	Reaction time (h)	Product distribution (%)			Selectivity of 2,6-DMN	2,6-DMN yield (%)
		MN	DMN	TMN		
ZSM-5	1	55.4	36.7	7.9	24.6	4.94
	6	63.2	28.2	8.6	15.4	1.09
SAPO-11	1	53.2	40.8	6.0	24.9	6.96
	6	59.1	32.4	8.5	36.5	3.50
ZSM-5/SAPO-11	1	52.7	42.2	5.1	27.2	7.85
	6	57.3	33.5	9.2	38.3	4.62
ZSM-5&SAPO-11	1	53.9	38.3	7.8	24.5	5.46
	6	62.1	30.9	7.0	15.7	2.32

Table 4 summarizes the product distributions of the methylation of naphthalene over synthesized samples. As shown in Table 4, the main products include methylnaphthalene (MN), dimethylnaphthalene (DMN) and trimethylnaphthalene (TMN). Table 4 shows that the selectivity of 2,6-DMN increases following the sequence ZSM-5/SAPO-11 > SAPO-11 > ZSM-5&SAPO-11 > ZSM-5, which is not consistent with the acidity of the samples, which indicates that the selectivity of 2,6-DMN and the acidity of synthesized samples are not explicitly linked to each other. Table 3 shows that the pore size of ZSM-5 is 0.63 nm, which is near to the kinetic diameter of the naphthalene molecule (0.62 nm), so ZSM-5 could inhibit the naphthalene molecule from entering into the pore channels, thus the selectivity of 2,6-DMN of ZSM-5 is the lowest in all the samples. However, ZSM-5/SAPO-11 possesses suitable pore size, which make it more favorable to the diffusion of reactions and products, thus finally leading to higher selectivity of 2,6-DMN. In addition, the 2,6-DMN yield decreases in the order of ZSM-5/SAPO-11 > SAPO-11 > ZSM-5&SAPO-11 > ZSM-5. So the catalytic performances of ZSM-5/SAPO-11 are the highest in all the samples.

ZSM-5/SAPO-11 reusability for 2,6-DMN synthesis

The catalytic performance of the reused ZSM-5/SAPO-11 catalyst is given in Table 5, it is seen that the experimental results decrease gradually. Generally, the main reasons for catalyst deactivation are the decrease of surface area and the loss of active species. Further the deep-seated reason is because water is generated during the methylation of naphthalene with methanol, leading to the structure collapse by dealumination of the catalyst by high temperature steam or even by the methanol itself.

Table 5 Reusability of ZSM-5/SAPO-11 catalyst

Times of reusability	Reaction time (h)	Conversion (%)	Selectivity (%)	Yield (%)
1	1	55.8	25.4	7.23
	6	24.1	34.2	4.12
2	1	41.2	20.3	5.45
	6	15.3	29.8	3.20
3	1	20.7	16.5	4.16
	6	9.4	23.7	2.60

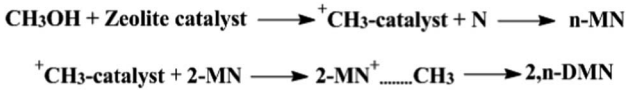

Fig. 10 Reaction mechanism of the methylation of naphthalene with methanol.

Reaction mechanism

The reaction mechanism of the methylation of naphthalene with methanol is shown in Fig. 10. To our knowledge, the methylation reaction is an acid-catalysed reaction, the carbocation is first produced by the reaction of the acid site (the active site) of zeolite catalyst and methanol. The next step is that the carbocation would attack the naphthalene molecule, and the *n*-MN are obtained. Then the carbocation continues to attack 2-MN, 2,*n*-DMN are prepared finally. And the formation of the carbocation is the key step, which affects the speed of the reaction.

Conclusions

In this paper, ZSM-5 (core)/SAPO-11 (shell) composite zeolite catalyst was prepared by hydrothermal method and tested in the methylation of naphthalene with methanol. In order to be compared, the mechanical mixture was prepared through the blending of ZSM-5 and SAPO-11. Also the physicochemical properties of synthesized samples were characterized by XRD, SEM, TEM, FT-IR, and so on. The XRD results showed that ZSM-5/SAPO-11 exhibited typical characteristic peaks of ZSM-5 and SAPO-11. The SEM and TEM analysis results indicated that the composite had the morphology with ZSM-5 as the core and SAPO-11 as the shell. The composite had more mesopores favorable for the diffusion of substances and suitable acidity distribution advantageous, which was helpful to increasing the catalytic performances.

Meanwhile, the composite showed relatively higher stability. Thus, the ZSM-5/SAPO-11 composite molecular sieve showed high catalytic performances in the methylation of naphthalene with methanol.

Conflicts of interest

There are no conflicts to declare.

Acknowledgements

The authors acknowledge the financial support from Fundamental Research Program for Young Scientists of Shanxi Province (Project No. 202103021223294), Fundamental Research Program of Shanxi Province (Project No. 202203021211203), Scientific and Technological Innovation Programs of Higher Education Institutions in Shanxi (Project No. 2020L0366), Key R& D Projects of Shanxi Province (Project No. 201903D121025), Key R& D Projects of Shanxi Province (Project No. 201903D221066), Taiyuan University of Science and Technology Scientific Research Initial Funding (Project No. 20182015 and 20182022), Shanxi Key Laboratory of High Value Utilization of Coal Gangue (Project No. 202104010910004), Key Research and Development Program of Shanxi province (Project No. 202102090301026), College Student Innovation and Entrepreneurship Training Project of Higher Education Institutions in Shanxi (Project No. 20210492, 20210493 and S20221010937), Innovation and Entrepreneurship Training Program for Undergraduate, Taiyuan University of Science and Technology (Project No. XJ2020045, XJ2021047, XJ2021051 and XJ2022049), and Excellent Innovation Project for Graduate Students in Shanxi Province (Project No. 2022Y707).

References

1 D. Tsakona, I. Theodorakos, A. Kalaitzis and I. Zergioti, *Appl. Surf. Sci.*, 2020, **513**, 145912–145918.
2 P. Slepička, O. Neděla, P. Sajdl, Z. Kolská and V. Švorčík, *Appl. Surf. Sci.*, 2013, **285**, 885–892.
3 D. Qian, S. Michelina, L. Nadia, C. Dario and A. René, *Chin. J. Polym. Sci.*, 2020, **38**, 311–322.
4 B. Du, Y. Gao and Z. X. Huo, *J. Electrost.*, 2009, **67**, 22–26.
5 X. X. Wang, Z. M. Liu, F. Guo, Y. C. Wang, X. X. Wei, P. Li, Y. B. Xue, Y. Y. Wang, S. Q. Guo and Y. Yu, *RSC Adv.*, 2018, **8**, 243–250.
6 C. Li, L. F. Li, W. Wu, D. S. Wang, A. V. Toktarevc, O. V. Kikhtyaninc and G. V. Echevskiic, *Procedia Eng.*, 2011, **18**, 200–205.
7 S. J. Kim, *J. Ind. Eng. Chem.*, 2019, **79**, 146–153.
8 J. H. Li, Q. Gang, H. Lian, L. F. Ding, Z. H. Hu and Z. R. Zhu, *J. Catal.*, 2019, **378**, 144–152.
9 Y. Ishigaki, K. Asai, H. P. J. D. Rouville, T. Shimajiri, V. Heita, H. Fujii-Shinomiya and Y. Suzuki, *Eur. J. Org. Chem.*, 2021, 990–997.
10 V. I. Bogdan, A. E. Koklin and V. B. Kazanskii, *Kinet. Catal.*, 2010, **51**, 736–742.
11 X. X. Wang, Z. M. Liu, X. X. Wei, F. Guo, P. Li and S. Q. Guo, *Braz. J. Chem. Eng.*, 2017, **34**, 295–306.
12 X. X. Wang, F. Guo, X. X. Wei, Z. M. Liu, W. Zhang, S. Q. Guo and L. F. Zhao, *Korean J. Chem. Eng.*, 2016, **33**(7), 2034–2041.
13 M. Liu, W. Wu, O. V. Kikhtyanin, L. F. Xiao, A. V. Toktarev, G. L. Wang, A. J. Zhao, M. Y. Smirnova and G. V. Echevsky, *Microporous Mesoporous Mater.*, 2013, **181**, 132–140.
14 Y. M. Fang and H. Q. Hu, *Catal. Commun.*, 2006, **7**, 264–267.
15 X. F. Bai, K. Y. Sun, W. Wu, P. F. Yan and J. Yang, *J. Mol. Catal. A: Chem.*, 2009, **314**, 81–87.
16 X. J. Dai, Y. Cheng, Q. Wei, M. Si, P. F. Zhang and Y. S. Zhou, *Microporous Mesoporous Mater.*, 2022, **343**, 112025–112040.
17 X. J. Dai, Y. Cheng, Q. Wei, M. Si and Y. S. Zhou, *Fuel*, 2022, **324**, 124610–124622.
18 X. M. Li, S. T. Tsai, K. C. W. Wu, O. J. Curnow, J. K. Choi and A. C. K. Yip, *Microporous Mesoporous Mater.*, 2021, **328**, 111475–111484.
19 S. Y. Li, H. H. Yang, S. Wang, M. Dong, J. G. Wang and W. B. Fan, *Microporous Mesoporous Mater.*, 2022, **329**, 111538–111548.
20 J. F. Li, K. Zhang, P. Liu, J. G. Wang, W. B. Fang, S. Wang, P. F. Wang, Z. F. Qin, Y. Y. Y. Chen and M. Dong, *ACS Catal.*, 2019, **8**, 5485–5505.
21 Q. M. Wu, X. Wang, G. D. Qi, Q. Guo, S. X. Pan, X. J. Meng, J. Xu, F. Deng, F. T. Fan, Z. C. Feng, C. Li, S. F. Maurer, U. Müller and F. S. Xiao, *J. Am. Chem. Soc.*, 2014, **136**, 4019–4025.
22 S. J. Xie, S. L. Liu, Y. Liu, X. J. Li, W. P. Zhang and L. Y. Xu, *Microporous Mesoporous Mater.*, 2009, **121**, 166–172.
23 Y. H. Zhang, Y. C. Liu and Y. X. Li, *Appl. Catal., A*, 2008, **345**, 73–79.
24 H. J. Chae, Y. H. Song, K. E. Jeong, C. U. Kim and S. Y. Jeong, *J. Phys. Chem. Solids*, 2010, **71**, 600–603.
25 X. Zhang, J. W. Wang, J. Zhong, A. Liu and J. K. Gao, *Microporous Mesoporous Mater.*, 2008, **108**, 13–21.
26 P. Wang, B. J. Shen and J. S. Gao, *Catal. Commun.*, 2007, **8**, 1161–1166.
27 X. X. Wang, S. Q. Guo, W. Zhang and L. F. Zhao, *J. Mol. Catal.*, 2013, **27**, 295–306.
28 J. Wen, G. Y. Wang, Y. Zhang, Z. G. Qiu and L. F. Zhao, *Pet. Technol.*, 2010, **39**, 487–491.
29 M. R. Agliullin, Z. R. Khairullina, R. Z. Kuvatova and B. I. Kutepov, *Catal. Ind.*, 2020, **12**, 89–94.
30 O. G. Somani, A. L. Choudhari, B. S. Rao and S. P. Mirajkar, *Mater. Chem. Phys.*, 2003, **82**, 538–545.
31 L. Han, Y. X. Liu, F. Subhan, X. M. Liu and Z. F. Yan, *Microporous Mesoporous Mater.*, 2014, **194**, 90–96.
32 V. Nieminen, N. Kumar, T. Heikkilä, E. Laine, J. Villegas, T. Salmi and D. Y. Murzin, *Appl. Catal., A*, 2004, **259**, 227–234.
33 Z. R. Zhu, Q. L. Chen, Z. K. Xie, W. M. Yang and C. Li, *Microporous Mesoporous Mater.*, 2006, **88**, 16–21.
34 M. A. Camblor, A. Corma and S. Valencia, *Microporous Mesoporous Mater.*, 1998, **25**, 59–74.